FROM EXPERIENCE-BASED TO KNOWLEDGE-DRIVEN DESIGN: A CASE STUDY OF A 3D-PRINTED PRODUCT

Højeng-Swensson, Jakob;
Pisinger, Victor Mathias;
Juul-Nyholm, Herle Kjemtrup;
Legarth, Brian Nyvang;
Eifler, Tobias

Technical University of Denmark

ABSTRACT

In this paper, a case study of a redesign process for 3D-printed parts has been analysed. The purpose was to compare the implementation of specialist knowledge in hands-on engineering tasks with the previous experience-based approach. Here, specialist knowledge refers to systematic experimental work as a basis for Computer Aided Engineering (CAE). The case involves a set of compliant arms for an oil extraction device developed by a start-up company. Tensile tests of 3D printed dog-bone were performed to characterise the Young's modulus, tensile strength, and orthotropic behaviour of the material to build a material model based on Finite Element Analysis (FEA). With the material characteristics and three simple tests to estimate the optimisation constraints, the existing solution was disproven. Then, new solution candidates were generated and evaluated with input from the start-up company. The process resulted in a feasible solution as well as a reduction of maximum stress from 54MPa to 20MPa. The case highlights the value of specialist knowledge for characterisation of new technologies and design space constraints to reduce and improve iterations to solve a practical design problem.

Keywords: Simulation, Design practice, Design process, Case study, 3D printing

Contact:
Juul-Nyholm, Herle Kjemtrup
Danmarks Tekniske Universitet / Technical University of Denmark
Denmark
hbaju@mek.dtu.dk

Cite this article: Højeng-Swensson, J., Pisinger, V. M., Juul-Nyholm, H. K., Legarth, B. N., Eifler, T. (2023) 'From Experience-Based to Knowledge-Driven Design: A Case Study of a 3D-Printed Product', in *Proceedings of the International Conference on Engineering Design (ICED23),* Bordeaux, France, 24-28 July 2023. DOI:10.1017/pds.2023.196

1 INTRODUCTION

In literature, product design is described as the task of developing a well-defined solution to a poorly defined problem (Cross, 2008; Design Council, 2007). While initially facing an undefined, perhaps even infinite, solution space (Cross, 2008), a design task implies finding a first abstract idea, and to gradually concretise it into a physical product that fulfills the specified requirements. In order to control the complexity of this task, literature provides several process models that structure the design process into subsequent design phases, e.g. *Task Clarification*, *Conceptual Design*, *Embodiment Design*, and *Detail Design* as suggested by Pahl and Beitz (2007). The purpose includes teaching novice engineers, delimiting the wide variety of activities in a design process from initial idea and concept generation to detailed documentation and production ramp-up, and managing an efficient design process through different milestones (Pahl and Beitz, 2007; Ullman, 2017).

At the same time, product design has evolved into a more multidisciplinary task due to the rapid technological development over the last decades. This evolution requires engineers to bring a multitude of different perspectives together throughout the design process (Isaksson and Eckert, 2020). Examples are the design of cyber-physical systems, the integration of machine learning and artificial intelligence, the growing importance of nanotechnologies, and designing products for new production technologies. As a result, product design changes from the gradual improvement of long-existing solutions, e.g. McMahon (1994), towards the integration of numerous, quickly evolving, technologies in complex assemblies.

For the future role of a design engineer, this implies that one of the key skills is to systematically combine specialist knowledge from an increasingly wide range of domains (Isaksson and Eckert, 2020), all while maintaining the ability to make successful design decisions on different levels of abstraction. What is less well described, however, is the question how available design and ideation methods such as brainstorming, morphological charts, etc. (Daly and Gonzalez, 2016) integrate with these new requirements for technical details. In other words, how an increased level of specialist knowledge will impact design practices and design decision making. After all, a complete characterisation of all relevant technological aspects, for example by means of physical experimentation or Computer Aided Engineering (CAE) approaches, will not be feasible as successful design in an industry context is essentially a time and resource constrained activity (Cross, 2008; Pahl and Beitz, 2007; Ullman, 2017).

Against this background, this paper takes a case-based perspective to investigate how technical specialist knowledge compares to the development process of a startup company, and provides insights for improved design practices. The company is developing an oil extraction device, which is predominately produced by additive manufacturing. The case was chosen as small- and medium-sized companies generally face high barriers of identification and implementation of new, specialist engineering tools (Robert et al., 2003). This also applies to the case company and the provided existing design, which was developed through an experience-based approach. Using the insights from the product development project in collaboration with the Technical University of Denmark (DTU), the paper provides an overview of how production and material type specialist knowledge (Cross and Sivaloganathan, 2007) in terms of material characterisation and Finite Element Analysis (FEA) affected design decisions, and how it was integrated with hands-on engineering work to deliver on the specified goals in the limited time frame, respectively. For this purpose, academic supervision focused mainly on the development of a suitable material model for the in-house available 3D printing process.

The remainder of the paper is organised as follows. Section 2 presents the case example, while section 3 describes the design process that was followed throughout the project including relevant results. On this basis, section 4 reviews the used design practices in order to discuss the influence of the initial characterisation of 3D printed parts, and whether the identified practices might be generalisable beyond the specific case. The paper closes with a discussion and an outlook to future work.

2 CASE EXAMPLE: OIL EXTRACTION DEVICE

The case concerns a sub-module of an oil extraction device. The device has been developed since 2017 and the first 50 pieces were sold in 2021 to field test the current iteration. It was discovered that the raising and locking mechanism for the glass container did not sustain a good contact between its glass container and the heating element during the oil extraction cycle. During the cycle, vacuum is created after the glass has been mounted, which offsets the glass from its original mounting position, see Fig. 1 a). This issue triples the oil extraction time and hence degrades the user experience and the

https://doi.org/10.1017/pds.2023.196 Published online by Cambridge University Press

value of the product. Therefore, the project team were asked to redesign the 3D printed compliant arms to ensure continuous contact between glass and heating plate during the oil extraction cycle. The project team was chosen due to their specialist knowledge on CAE, which was not available in the company, where rapid prototyping had been the means for development.

a) A gap appears between the glass and the heating plate during operation, here illustrated by the black sheet pushed in as shown in the circle.

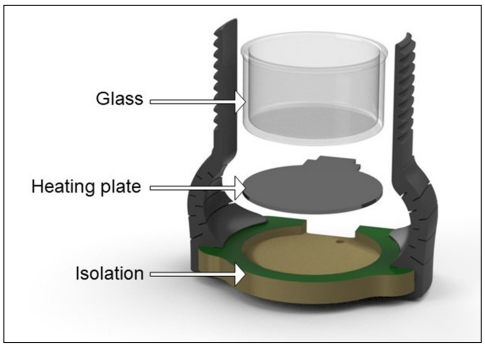

b) Exploded view of the glass mounting assembly with the compliant arms at the sides and the stack of the glass, heating plate and isolation in the middle.

Figure 1. Illustrations of the problem for the original oil extractor design: Challenges with sustaining a good contact between glass and heating plate.

The company uses a Prusa i3 MK3S+ 3D printer, which is based on the fused deposition modeling (FDM) technology, with polyethylene terephthalate glycol (PETG). Due to the nature of the 3D printing process with solid shell, bottom/top print, and reduced density infill, the mechanical properties of the produced parts are different than injection molded parts. As a reference, unfilled PETG has a Young's modulus of $E = 2.05$GPa and a tensile strength of $\sigma_{max} = 63$MPa. Due to the company's choice of production method, the requirements for the solution were that:

- It should be 3D printed in PETG with the company's standard settings,
- It should not be relying on support nor brim in printing,
- It should fit the current design of the other components.

Further requirements and technical constraints regarding the glass mounting issue were not given.
The project team had contact with the company throughout the project as well as an academic supervision team. The contact to the company gave them the chance of getting all available information during the process as well as direct feedback on prioritisation questions and solutions, ensuring the link between the academic purpose of the project and the practical context. Part of this practical context was the use of 3D printing as a new production technology, which offers new opportunities and challenges in terms of form and function of mechanical parts.

3 THE DESIGN PROCESS

3.1 Material experiments

The first process step in redesigning the compliant arms was to perform material experiments. The purpose of the material experiments was to determine the Young's modulus, yield stress and level of orthotropy of the 3D-printed PETG to develop a material model for finite element modelling of the parts. The material properties were determined through tensile tests with basic dog-bone samples for a selection of printing directions. To model the strength of arbitrary orientated 3D printed parts, the tensile tests were performed for the main printing directions as well as the intermediate directions. Since the Poisson's ratio can be manipulated by the print infill structure, which is outside the present scope, the Poisson's ratio of moulded PETG, $\nu = 0.4$, was assumed.
Before the dog-bone tests were carried out, the dimensional precision variation between the printers was determined by printing six unit cubes (10x10x10mm) and measuring the variation. Then, the dog-bone samples were printed and tested according to ISO-527 part 1 and 2, which concerns plastic determination of tensile properties and test conditions for moulding and extrusion plastics, respectively. It is noted that there is currently no ISO-standard for testing 3D-printed material properties.

https://doi.org/10.1017/pds.2023.196 Published online by Cambridge University Press

Seven printing directions were examined with seven samples each, see Fig. 2 a). They were named according to their orientation, ⟨u,v,w⟩, which represents the rotation about x, y, and z, respectively. The samples were printed on two different printers using the same printer settings, but with each direction on the same printer due to size and timing. The force-displacement curve were measured using the tensile test machine (Instron 5965) and the strain was measured using an extensometer. The tensile tests were performed until fracture or up to 2.3mm displacement (about 2% strain) for each the test samples.
The Young's modulus measurements are shown in Fig. 2 c) and the linear regression results are shown in Tab. 1 with the mean results for the tensile strength. All of the directions show significantly lower Young's modulus and tensile strength than unfilled PETG ($E = 2.05$GPa and $\sigma_{max} = 63$MPa). The variation in Young's modulus is small for the majority of directions. The Young's modulus of ⟨0,45,45⟩ is significantly lower, and the ⟨45,0,0⟩ and ⟨90,0,0⟩ are significantly higher. The spread of the ⟨0,45,45⟩ direction makes it difficult to determine its actual value and its deviation from the mean.
Since there is no significant difference between ⟨0,0,0⟩ and ⟨0,0,45⟩, it was concluded that the process is symmetric in the printing plane. However, it is hard to conclude anything on orthotropy due to printer variation and the low number of data points. It was assumed that the difference between ⟨0,0,0⟩ and ⟨90,0,0⟩ is due to difference in printer paths between top/bottom layers and vertical shells as illustrated in Fig. 2 b). The influence of symmetry, infill type, fiber binding and printing on a raft was investigated on a qualitative basis, but the result are not reported here.

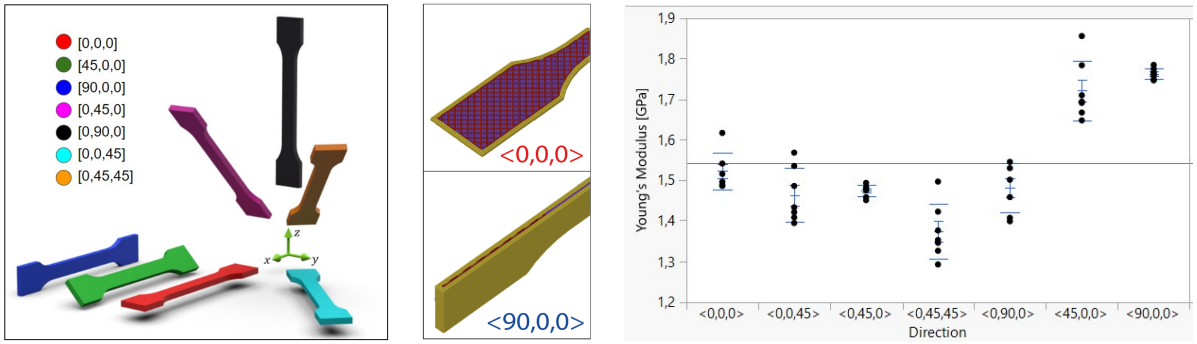

a) Definition of dog-bone 3D print directions.

b) Examples of print direction.

c) Young's modulus results for all print directions.

Figure 2. Dog-bone 3D print directions, print examples and Young's modulus results.

Table 1. Material test results from linear regression.

Direction	⟨0,0,0⟩	⟨45,0,0⟩	⟨90,0,0⟩	⟨0,45,0⟩	⟨0,90,0⟩	⟨0,0,45⟩	⟨0,45,45⟩
Young's modulus [GPa]	1.52	1.72	1.76	1.48	1.48	1.46	1.37
Tensile strength [MPa]	29.4	31.7	33.4	20.9	15.7	27.2	24.9

3.2 Material model

Based on the tests described in Sec. 3.1, the material model was developed based on parameterised local search heuristics for finite element simulations. Isoparametric elements were used for the modelling and due to the risk of inadequate mesh refinement, some noise was expected in the optimisation. This was considered when a modified Newton-Raphson method was chosen for the optimisation heuristic.
The complexity of the model evolved over three iterations. First, a linear isotropic material model with infill modelling as illustrated by the simple material decomposition in Fig. 3 a) was developed. Here, it was assumed that the Young's modulus of the infill is directly proportional to the infill percentage.
For the linear model, it was assumed that the material has a Young's modulus equal to the average Young's modulus of the corresponding printing direction. In the finite element model, the samples were fully clamped at one end and only unconstrained for axial deflection in the other. The loads were modelled as lumped nodal loads in the end where axial deflection is allowed, and the loads of 0.1kN to 1kN were applied in steps of 0.1kN. The constraints and loads were applied to the same areas as the tensile test machine.

https://doi.org/10.1017/pds.2023.196 Published online by Cambridge University Press

In Fig. 3 b), the force error of the linear isotropic model relative to the experiments as a function of the strain is shown. The model produces an error bigger than the printer variation. Especially the directions ⟨45,0,0⟩ and ⟨90,0,0⟩ are not modelled accurately using the linear isotropic material model.
In the second iteration, a nonlinear material model, also with the simple material decomposition of Fig. 3 a), was developed. It performed slightly better than the linear one, but is not shown here.

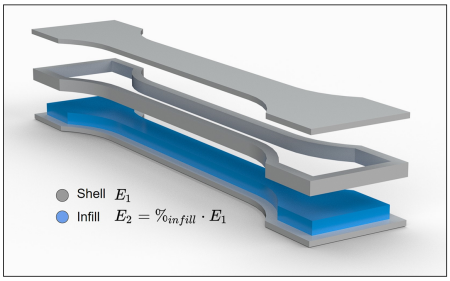

a) Material decomposition with shell and infill.

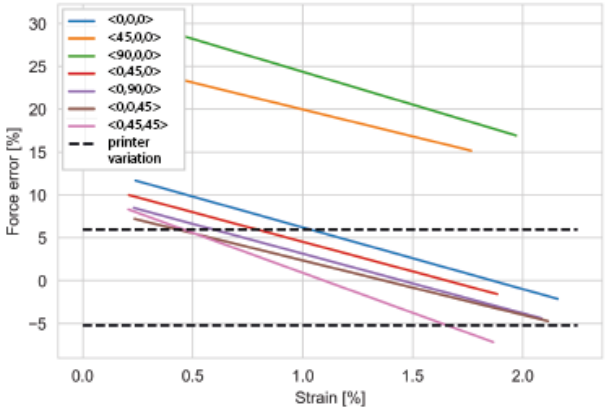

b) Force error as a function of strain for linear material model.

Figure 3. Linear material model with simple material decomposition.

In the third iteration, an advanced material model was developed with six printing type volumes as illustrated in Fig. 4 a). In the tensile tests, there is a clear difference in strength between top/bottom and shell layers. Also, the strength was degraded when printing the specimens on a raft. This means that apart from the linear and quadratic terms of the Young's modulus for top/bottom, infill and shell layers, the linear and quadratic terms for vertical printing needed to be determined. The six volumes were chosen to better reflect the properties of the different printing directions and the Young's modulus was assigned according to these directions.
The force error of the advanced model relative to the experiments can be seen in Fig. 4 b). The optimisation algorithm had some convergence issues and did not adjust the quadratic terms, but still resulted in a model with force errors within the printer variation. The algorithm found a difference between the shell layers and the bottom/top layers as expected, which is needed to estimate the effect of different 3D-printed shell thickness.

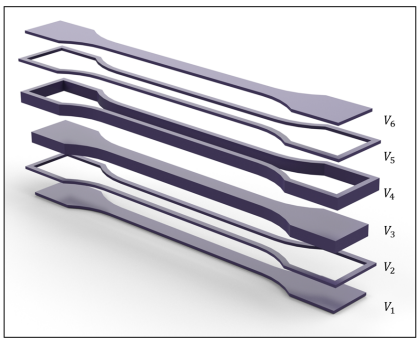

a) Material decomposition with six printing type volumes.

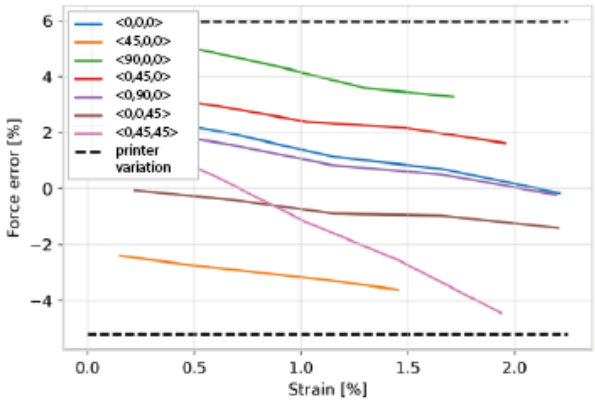

b) Force error plot for advanced material model.

Figure 4. Advanced material model with six-volume material decomposition.

https://doi.org/10.1017/pds.2023.196 Published online by Cambridge University Press

To validate the material model, tensile tests and finite element analyses were conducted for the current compliant arm design. The tensile tests were performed with four samples printed on two different printers for a total of eight experiments. The setup can be seen in Fig. 5 a). The results of the five successful experiments are represented by the lines in Fig. 5 c). The finite element analysis was set up as illustrated in Fig. 5 b). Furthermore, the shape was divided into four volumes corresponding to the printed shell, top/bottom layer and infill. The results of the simulations can be seen in Fig. 5 c) as the dark blue dots. The red and light blue dots represent the simulation results for the linear isotropic material model using the highest and lowest Young's modulus from the material tests.
It is seen that for low displacements the advanced material model preforms better than the linear isotropic models, but at higher displacements the model deviates from the measured results. The deviation is probably due to the material profiles quadratic term not being adjusted during optimisation. From above evaluation of the linear model (illustrated in Fig. 3 b) it is clear that the average linear material model is unable to model the tensile test samples even though a linear model with a mean Young's modulus might seem more suitable when looking at the comparison. Another argument for not using the linear isotropic material model, is that the model does not include the difference between the layer types. The difference in layer types is extremely useful when optimising parts, as this expands the feasible solution space, resulting either in components with less stressed regions and/or more tolerance to aesthetic design changes.

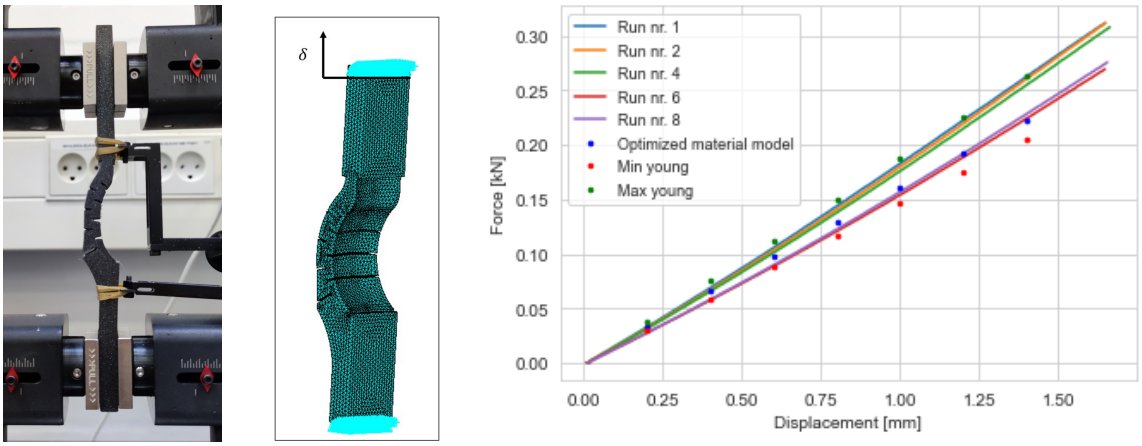

a) Physical experiment.

b) Simulation experiment.

c) Comparison of physical (lines) and simulation experiment (dots).

Figure 5. Setup of physical and simulation experiments and comparison of the two.

3.3 Optimisation constraints

The given requirements were all qualitative and hence did not define the constraints on the parametric design space of the compliant arm design. As these constraints were needed for the exploration and optimisation of the design through finite element analysis, it was decided that rapid and simple experimentation with few repetitions and additional safety factors were sufficient.
Three experiments were set up to estimate the vacuum seal force, the liquid seal force and the glass displacement during vacuum generation. The test setups can be seen in Fig. 6.
To estimate the minimum force needed to sustain a vacuum, the machine's ability to generate a vacuum was tested with the setup pictured in Fig. 6 a). It shows the oil extraction machine upside down, with the glass but without the compliant arms. On top of the glass different masses were placed and the vacuum generation was tested. Part of the results can be seen in Tab. 2. It was concluded that the machine was able to create a vacuum if the force between the glass and the gasket was above 2.5N. Adding an arbitrary safety factor, the constraint was set to 3N.

Table 2. Vacuum seal force test results.

Vacuum seal force [N]	0.51	1.65	2.14	2.29	2.52	2.54
Vacuum Evaluation	Failed	Failed	Failed	Failed	Passed	Passed

https://doi.org/10.1017/pds.2023.196 Published online by Cambridge University Press

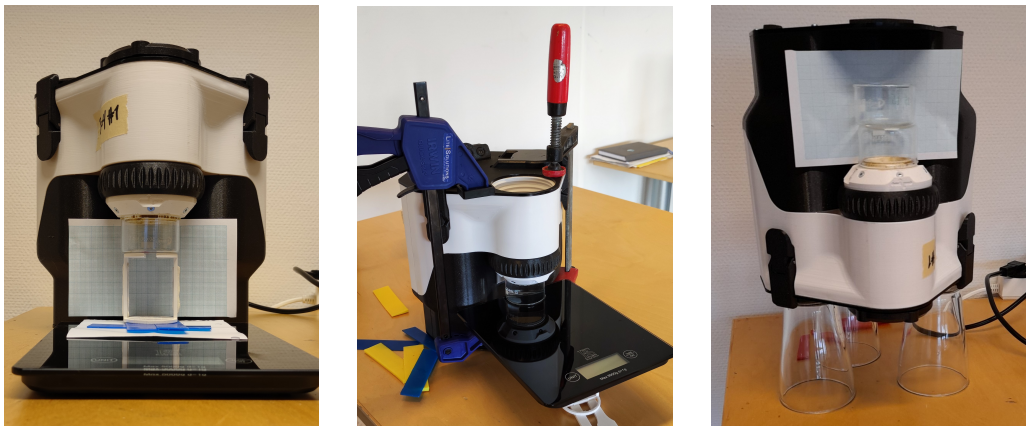

a) Vacuum seal force. b) Liquid seal force. c) Glass displacement.

Figure 6. Pictures of test setups.

To estimate the minimum force to seal the glass from leaking if the vacuum is lost, the glass was placed on a scale held in place by clamps. The clamps were tightened to about 48N to guarantee a tight seal. Then the glass was filled completely with liquid and the clamps were loosened in steps between 1 and 10N. The test was performed with both water and isopropanol as isopropanol have a higher probability of leaking and is used in the extraction process. The results can be seen in Tab. 3. The average force is 21N. The constraint was set to 25N by adding an arbitrary safety value.

Table 3. Liquid seal force test results.

Test	Water	Water	Isopropanol	Isopropanol	Average
Liquid seal force [N]	17	25	19	24	21

To estimate the displacement of the glass due to the creation of vacuum, the glass was placed on a simple support frame on top of a scale. Using a plastic wedge under the frame, the read out on the scale was set to 310±10g to achieve the necessary force of 3N for the vacuum seal. Millimeter-paper was placed behind the glass and the process of generating vacuum was recorded on a video. In Fig. 7, the displacement as a function of time is shown as a result of measuring the bottom of the glass relative to a fixed point on the millimetre-paper in the video. The maximum displacement was estimated to 1.05mm considering the video quality. With an arbitrary safety value, the constraint was set to 2mm.

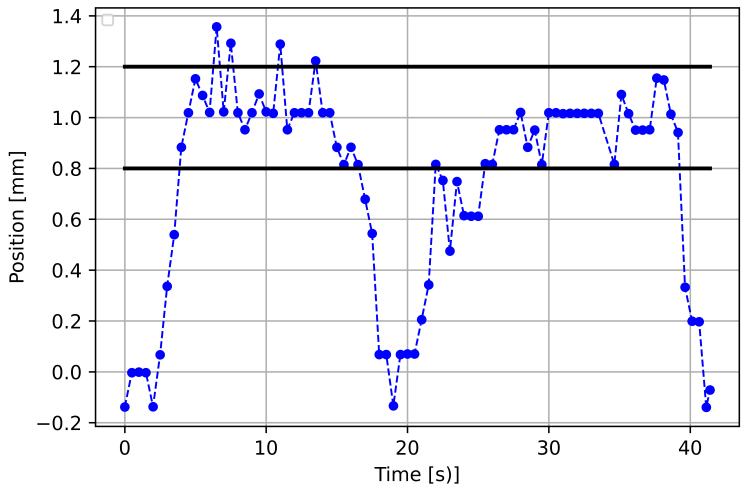

Figure 7. Glass displacement measurements during two vacuum cycles as a function of time.

https://doi.org/10.1017/pds.2023.196 Published online by Cambridge University Press

3.4 Ideation & optimisation

The finite element analysis of the existing solution gave some important insights for the redesign. By looking at the Mises stress distribution in Fig. 8, it was observed that the cut notches did not result in the intended compliance to accommodate the displacement but rather in large stress accumulations. Based on analytical estimates, it was concluded that the solution space of the existing compliant arms with regards to the compliance constraints from Sec. 3.3 was very small.

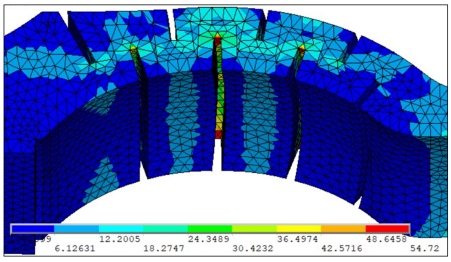

Figure 8. Mises stress distribution for existing solution, $\sigma_{max} = 54MPa$.

Alternative solutions were generated based on the requirements, the experience from the material tests and the experience from the production at the company. Three designs, an *Omega shape*, a *Scissor shape*, and a *Multi curve shape*, were chosen for quantitative evaluation and comparison. The comparison was based on parametric optimisation with the objective of minimising the maximum stress, $min(\sigma_{max})$, due to the poor strength to stiffness ratio of the material, PETG. The designs were parametrised by 3-4 parameters each. In the analysis, the designs were clamped at one end and the displacement of 2mm were applied at the other. Then a force of 25N was applied in addition to the reaction forces to ensure the liquid seal. For Scissor and Multi curve designs, the number of compliant sections were varied.

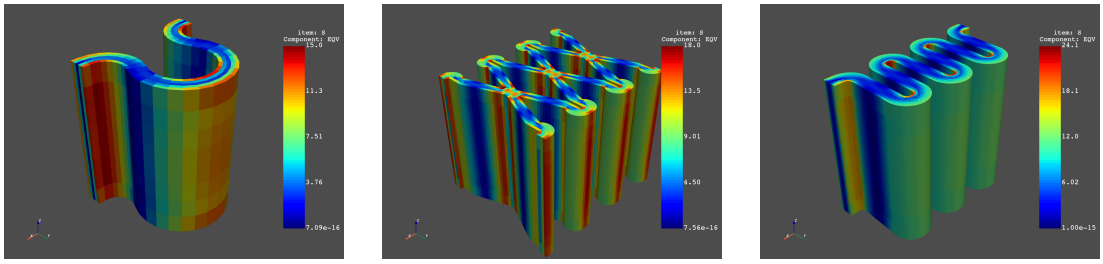

a) Omega shape, $\sigma_{max} = 15$MPa.

b) Scissor shape, $\sigma_{max} = 18$MPa.

c) Multi curve shape, $\sigma_{max} = 24$MPa.

Figure 9. Shape candidates for redesign of the compliant arms.

The local optima for the three designs can be seen in Fig. 9. It can be seen that the Omega shape has the lowest peak stress of 15MPa, the Scissor shape a little higher on 18MPa, and the Multi curve shape has the highest of 24MPa. Looking at the stress distribution for the scissor shape, it is observed that the stress peaks are in the stress relievers at the outer intersections. This might prove to be a problem due to the inevitable variation between printers as it is very sensitive to changes in the radius and therefore could be challenging to produce. For the Omega shape the peak stress is mainly on the inside of the curves. For the curves at the end the real world mounting is different meaning these can be neglected. For the radius in the middle the peak stress happens at the edges, which can be resolved by removing a bit of material at the edge of the inner central curve. Hence, there is a bigger potential for reducing the stress of the omega shape than the scissor shape. The omega shape is also preferred due to print-ability, ease of use and ability to convert into a visually pleasing design.

The next step was to adjust the omega shape to the interfaces on the machine. Two alternatives were optimised for the minimum maximum stress, $min(\sigma_{max})$, and compared. The CAD illustrations and stress plots can be seen in Fig. 10. Omega design A is better in terms of the peak stress of 16MPa compared

https://doi.org/10.1017/pds.2023.196 Published online by Cambridge University Press

to 20MPa, which is only achievable for Omega design B after minor adjustments of the inner edges of the horizontal mount and by neglecting the badly modelled mounting feature. On the other hand, Omega design A takes up more printing space and material, which is of big concern for the company. In addition to this, the visual appeal of the Omega design B compared to Omega design A, contributed to the choice of Omega design B as the final design as can be seen in Fig. 11. In the end, the commercial viability was prioritised over the technical objective from the company's side, This was based on the assumption that both alternative could pass a functional test. This was also the case; Omega design B passed a final vacuum and displacement test.

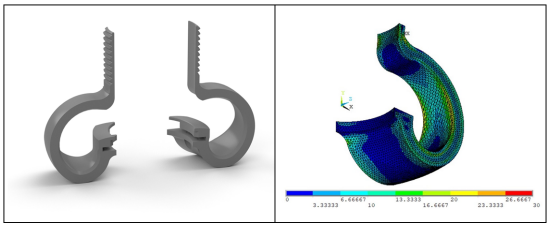

a) Omega design A, $\sigma_{max} = 16$MPa.

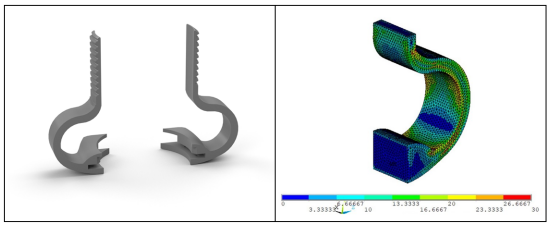

b) Omega design B, $\sigma_{max} = 20$MPa after minor adjustments at inner edges.

Figure 10. Final candidates for the redesign of the compliant arms.

Figure 11. Final redesign of the compliant arms without gap between heating plate and glass.

4 KEY INSIGHTS

From the structure of the design process described in Sec. 3, it is clear that the development of the redesign is based on the specialist knowledge of material experiments and model development. These two first steps allow for characterisation of 3D printing as a new production technology, even though it does not yet have a specific ISO-standard for testing.

As shown in the beginning of Sec. 3.4 and Fig. 8, the first valuable gain of the specialist knowledge in relation to the traditional design process was that it allowed for a detailed evaluation of the existing solution by means of CAE. Having the maximum stress of this design as a benchmark and having an explanation for why it did not work as intended was a valuable starting point for successful redesign.

Secondly, the experiments contributed with qualitative knowledge about print settings and properties, which was used to guide the ideation and choice of candidate designs. With the gained knowledge, the candidate designs were already feasible in regards to printing direction, size, and settings, which was one the requirements from the company.

After this, the solution candidates could be explored in detail using quantitative methods, i.e. through optimisation of the maximum stress using both the material model and the constraints from Sec. 3.3. The efficient exploration of the parametric design space made it possible to converge to a fully functional solution with $\sigma_{max} = 20$MPa compared to the initial solutions with $\sigma_{max} = 54$MPa, which at the same time violated the functional constraints for the vacuum seal.

The authors acknowledge that the input from the company represents the necessary counter-balance of the specialist knowledge. Without the given requirements coming from the practical and strategic perspective as well as the qualitative evaluation of the visual appearance and commercial viability of the candidate solutions, the final redesign would not have been feasible in the industrial context.

https://doi.org/10.1017/pds.2023.196 Published online by Cambridge University Press

5 DISCUSSION & CONCLUSION

Looking at the project as a case of implementation of specialist knowledge in a small company, other insights become important too. One interesting detail is that the optimisation of the advanced material model did not converge. Taken from the results, it still proved to be more useful than an experience-based approach. Another interesting aspect is the simplicity of the optimisation constraint experiments. In an academic setting they would not have been valid, but for the practical purpose at hand they provided enough information to develop a solution that could pass the final test.

Admittedly, the specialists were not implemented in the company as such, but the project team worked with the company and took part in both the specialist tasks and the subsequent design tasks. This meant that the knowledge gained through the exploratory material tests could be employed for ideation. In other words, by doing the experiments and exploring the optimisation constraints, empty design spaces was ruled out quickly, the number of iterations was reduced, valuable time was saved, and the company was satisfied with the result.

Returning to the comparison of the processes, the application of CAE as opposed to the experience-based approach allowed for a detailed disproof of the existing solution. Understanding why a solution does not work and how far it is from the limit, e.g. maximum stress in relation to yield stress, is much more valuable than just knowing that it fails. In addition to numerical optimisation, the evaluation of solution candidates and refinements also benefit from detailed quantitative evaluation and could be extended beyond stress considerations.

Concluding on the case study, the use of specialist knowledge significantly improved the solution by reducing the maximum stress and fulfilling the sealing constraints. In a more scientific approach this could be extended to a more structured definition and exploration of design spaces including technological constraints and multiple objectives. This would allow for a more computational design approach with an early focus on avoiding constraints and optimising for the objectives (Papalambros and Wilde, 2000; Clausing and Frey, 2005).

ACKNOWLEDGMENTS

The authors would like to thank Drizzle Aps for sharing design information and data.

REFERENCES

Clausing, D. and Frey, D. (2005), "Improving system reliability by failure–mode avoidance including four concept design strategies", *Systems engineering*, Vol. 8 No. 3, http://doi.org/10.1002/sys.20034.

Cross, M. and Sivaloganathan, S. (2007), "Specialist knowledge identification, classification, and usage in company-specific new product development processes", *Proceedings of the Institution of Mechanical Engineers, Part B: Journal of Engineering Manufacture*, Vol. 221 No. 8, http://doi.org/10.1243/09544054JEM580.

Cross, N. (2008), *Engineering design methods — strategies for product design*, 4 edition.

Daly, S.R., S.C.Y.S. and Gonzalez, R. (2016), "Comparing Ideation Techniques for Beginning Designers", *Journal of Mechanical Design*, Vol. 138 No. 10, http://doi.org/10.1115/1.4034087.

Design Council (2007), *Eleven lessons: managing design in eleven global companies*, Technical Report 272099.

Isaksson, O. and Eckert, C. (2020), *Product Development 2040: Technologies are just as good as the designer's ability to integrate them*, Technical Report September, Design Society Report DS107, http://doi.org/10.35199/report.pd2040.

McMahon, C.A. (1994), "Observations on modes of incremental change in design", *Journal of Engineering Design*, Vol. 5 No. 3, pp. 195–209, http://doi.org/10.1080/09544829408907883.

Pahl, G. and Beitz, W. (2007), *Engineering design — A systematic approach*, 3 edition, http://doi.org/10.1016/0261-3069(96)84970-3.

Papalambros, P. and Wilde, D. (2000), *Principles of optimal design: modeling and computation*, Cambridge university press.

Robert, J., Buhman, C., Garcia, S. and Allinder, D. (2003), "Bringing cots information technology into small manufacturing enterprises", in: H. Erdogmus and T. Weng (Editors), *COTS-Based Software Systems*, Springer Berlin Heidelberg, Berlin, Heidelberg, pp. 187–195, http://doi.org/10.1007/3-540-36465-X_18.

Ullman, D.G. (2017), *The mechanical design process*, McGraw-Hill New York, 6 edition.